Published in final edited form as:
Dev Biol. 2013 August 15; 380(2): 233–242. doi:10.1016/j.ydbio.2013.05.007.

Frazzled/DCC facilitates cardiac cell outgrowth and attachment during *Drosophila* dorsal vessel formation

Frank D. Macabenta[a,b], **Amber G. Jensen**[a,b], **Yi-Shan Cheng**[a], **Joseph J. Kramer**[a], and **Sunita G. Kramer**[a,b,*]

[a]Department of Pathology and Laboratory Medicine Robert Wood Johnson Medical School, University of Medicine and Dentistry of New Jersey, 675 Hoes Lane, Piscataway, NJ 08854, USA

[b]Graduate Program in Cell and Developmental Biology, UMDNJ-Graduate School of Biomedical Sciences & Rutgers, The State University of New Jersey, 190 Frelinghuysen Road, Piscataway, NJ 08854-8020, USA

Abstract

Drosophila embryonic dorsal vessel (DV) morphogenesis is a highly stereotyped process that involves the migration and morphogenesis of 52 pairs of cardioblasts (CBs) in order to form a linear tube. This process requires spatiotemporally-regulated localization of signaling and adhesive proteins in order to coordinate the formation of a central lumen while maintaining simultaneous adhesion between CBs. Previous studies have shown that the Slit/Roundabout and Netrin/Unc5 repulsive signaling pathways facilitate site-specific loss of adhesion between contralateral CBs in order to form a luminal space. However, the concomitant mechanism by which attraction initiates CB outgrowth and discrete localization of adhesive proteins remains poorly understood. Here we provide genetic evidence that Netrin signals through DCC (Deleted in Colorectal Carcinoma)/UNC-40/Frazzled (Fra) to mediate CB outgrowth and attachment and that this function occurs prior to and independently of Netrin/UNC-5 signaling. *fra* mRNA is expressed in the CBs prior to and during DV morphogenesis. Loss-of-*fra*-function results in significant defects in cell shape and alignment between contralateral CB rows. In addition, CB outgrowth and attachment is impaired in both *fra* loss- and gain-of-function mutants. Deletion of both Netrin genes (*NetA* and *NetB*) results in CB attachment phenotypes similar to *fra* mutants. Similar defects are also seen when both *fra* and *unc5* are deleted. Finally we show that Fra accumulates at dorsal and ventral leading edges of paired CBs, and this localization is dependent upon Netrin. We propose that while repulsive guidance mechanisms contribute to lumen formation by preventing luminal domains from coming together, site-specific Netrin/Frazzled signaling mediates CB attachment.

*Corresponding author at: University of Medicine and Dentistry of New Jersey, Department of Pathology and Laboratory Medicine, Robert Wood Johnson Medical School, 675 Hoes Lane West, Piscataway, NJ 08854, USA. Fax: +1 732 235 4825. kramersg@umdnj.edu (S.G. Kramer).

Appendix A. Supporting information

Supplementary data associated with this article can be found in the online version at http://dx.doi.org/10.1016/j.ydbio.2013.05.007.

Keywords

Drosophila; Dorsal vessel; Cardiac; Frazzled; DCC; Netrin

Introduction

Formation of the *Drosophila* dorsal vessel (DV) requires a highly stereotyped set of morphogenetic movements. During *Drosophila* cardiac morphogenesis, 104 cardioblasts (CB) are specified in two bilateral rows of cells that coordinately migrate towards the dorsal midline where they undergo cell polarity and shape changes, and make specific contacts across the dorsal midline to form the DV, a single cell-layer linear tube with a central lumen. The rows of CBs are flanked by two rows of non-muscle pericardial cells (PCs) shown to coordinate dorsal migration with the overlying ectoderm (Chartier et al., 2002). Similar to the primitive heart tube in vertebrates, the *Drosophila* DV possesses anteroposterior polarity and is subdivided, through the action of homeotic genes, into a narrower anterior portion called the aorta and a wider more posterior heart (Lo et al., 2002) (Fig. 1A). Within segments A2–A8, CBs can be subdivided into either smaller contractile cells that express the homeodomain gene *tinman*, or larger rounded cells expressing the orphan nuclear receptor seven-up (Gajewski et al., 2000). In the late stage embryonic DV, wingless (wg) expression in three segmentally repeated double pairs of CBs marks the differentiation of the seven-up positive CBs within the heart into the inflow tracts called ostia (Lo et al., 2002; Molina and Cripps, 2001).

The proper morphogenesis of the heart depends on the precise alignment of the two rows of CBs with each other at the dorsal midline. As the rows approach one another, each CB undergoes a series of dramatic cell shape changes and regulates its adhesive interactions with the opposing cell in such a way that they become attached at the dorsal-most and ventral-most points while maintaining a space in between (see Fig. 5). Cell contact and adhesion is first initiated dorsally, as each CB extends a leading edge towards its contralateral counterpart across the dorsal midline, resulting in an adhesive interaction. Subsequently, the CB extends a second leading edge to make a ventral connection with its counterpart. In this way, a sealed linear tube with a central lumen is formed (Medioni et al., 2008; Santiago-Martinez et al., 2008).

Guidance molecules and adhesion proteins have been shown to play a crucial role in the process of lumen formation. It was previously shown that in embryos mutant for the gene *shotgun*, which encodes *Drosophila* E-Cadherin (E-Cad), the adhesion between opposing CBs is defective resulting in the absence of lumen formation (Haag et al., 1999). Furthermore, our previous findings show that E-Cad localizes specifically to the dorsal and ventral attachment points and that this discrete localization is dependent upon negative regulation of E-Cad by the Slit/Robo pathway (Santiago-Martinez et al., 2008). In the absence of Slit/Robo signaling, E-Cad is no longer restricted to the dorsal and ventral attachment points and is found along the entire luminal domain. As a result, the CBs become fully attached, leading to a loss of luminal space (Medioni et al., 2008; Santiago-Martinez et al., 2008). Similarly, the Unc5 receptor, which mediates a repulsive response to the Netrin

guidance cue, also participates in lumen formation by providing repulsion of opposing CB membranes in a Slit/Robo-independent manner (Albrecht et al., 2011). However, while it is clear that repulsive guidance plays a role in establishing the luminal space between opposing CBs, it is still unknown what signal or signals are responsible for mediating CB outgrowth, extension and attachment.

Netrin was originally identified as a diffusible long-range Laminin-like extracellular axon guidance cue in *Caenorhabditis elegans* (Ishii et al., 1992). Subsequently, Netrins have been found in a wide range of animal species and have been shown to mediate guidance and cell adhesion in many different cell types (reviewed in (Lai Wing Sun et al., 2011)). Receptors for Netrins include the single-pass transmembrane proteins Deleted in Colorectal Cancer (DCC) and Unc5 (for review see (Lai Wing Sun et al., 2011). Different receptor combinations have been shown to elicit attractive or repulsive responses to Netrin via signaling pathways that ultimately result in the rearrangement of the actin cytoskeleton (Moore et al., 2007). In general, DCC mediates chemoattraction, while chemorepulsion requires Unc5 and in some cases DCC as well. More recently, the Down Syndrome Cell Adhesion Molecule (DSCAM) was also shown to function as both an attractive and repulsive Netrin receptor in *Drosophila* and vertebrates (Andrews et al., 2008; Ly et al., 2008; Purohit et al., 2012).

In *Drosophila*, DCC is called Frazzled (Fra) and was originally indentified as a receptor for the attractive Netrin guidance cue in the CNS (Harris et al., 1996; Kolodziej et al., 1996; Mitchell et al., 1996). DCC/Fra has been shown to mediate chemoattractive responses to Netrin in a variety of cell types (for a recent review see (Lai Wing Sun et al., 2011)). Additionally, more recent studies have shown that the DCC/Fra receptor becomes polarized on the cell membrane to the areas corresponding to asymmetric cell outgrowth and protrusion in a Netrin-dependent manner (Quinn and Wadsworth, 2008). For example, the polarized protrusive activity of the *C. elegans* HSN neuron is mediated by UNC-40 (*C. elegans* DCC) in response to a ventrally localized Netrin signal (Adler et al., 2006). Similarly, during *C. elegans* anchor cell invasion, localized Netrin secretion directs UNC-40 to a specific region of the anchor cell plasma membrane (Ziel et al., 2009). However, the precise role for Netrin in polarizing DCC/Fra is unclear, as recent evidence suggests that UNC-40 also has the ability to intrinsically polarize in the absence of UNC-6 (*C. elegans* Netrin) (Xu et al., 2009).

In this study, we show that the attractive Netrin receptor Fra is involved in mediating asymmetric CB outgrowth and attachment during DV morphogenesis. *fra* is expressed by the CBs, and genetic perturbation of *fra* levels results in a failure of CBs to properly come together at dorsal and/or ventral attachment points. Similar defects are observed in embryos mutant for Netrin or *fra, unc5* double mutants. Furthermore, we show that Fra accumulates at the sites of CB outgrowth and attachment and that this accumulation is correlated with proper lumen formation. Finally we show that Fra localization at sites of attachment is disrupted in embryos mutant for Netrin. Our findings provide evidence that just as repulsive guidance via the Robo and Unc5 receptors is important for preventing specific areas of the CB membranes from coming into contact, so too is attractive guidance via the Fra receptor for bringing together CBs at specific sites of adhesion.

Materials and methods

Fly stocks and genetics

Fly crosses were performed at 25 °C and maintained on standard medium. The following stocks were used: (*fra*^{3}) (BL#8813) and unc5 (*unc*5^{8}) (Labrador et al., 2005), Δ*NetAB* (Brankatschk and Dickson, 2006), *UAS-fra-myc* (G. Bashaw), *unc*5^{GS2}, *fra*^{3}/CyoWgBgal (G. Bashaw), 24*B-Gal*4 (Brand and Perrimon, 1993), *Hand-Gal*4 (Han et al., 2006), *UAS-mCD*8-*GFP* (BL#5130). To generate *fra* rescue embryos, *fra*^{3}/*CyO, twi-*2*XGFP; UAS-fra-myc* flies were crossed to *fra*^{3}/*CyO, twi-2XGFP*; 24*B-Gal*4 or *fra*3, *Hand-Gal*4/*CyO, twi-*2*xGFP flies*. For examining Fra-Myc localization in Δ*NetAB* mutants, FM7 sqh: :ChRFP; *UAS-fra-myc* males were crossed to Δ*NetAB/FM7-Kr-Gal*4, *UAS-GFP*;24*B-Gal*4 *females*. For *unc*5 dominant suppression experiments, *UAS-fra-myc* flies were crossed to *unc*5^{8}/*Cyo,KrGFP*; 24*B-Gal*4/TM6TB;Sb flies.

In situ hybridization

In situ hybridization on wild type and *Hand-Gal*4/*UAS-lacZ* embryos was performed as described (Lecuyer et al., 2008). For the *fra* antisense probe, the cDNA was linearized with BglII and transcribed using DIG RNA labeling mix (Roche Diagnostics). The Tyramide signal amplification kit was purchased from Molecular Probes. Double labeling was performed with a Rabbit anti-βgal antibody and a goat anti-Rabbit Alexa 555 secondary antibody.

Immunohistochemistry

Embryos were collected from grape-juice agar plates, dechorionated and fixed according to standard protocols. The following primary antibodies were used: rabbit anti-Mef2 (B. Paterson, 1:1000), rabbit anti-Myc (Sigma, 1:200), mouse anti-α-Spectrin [Developmental Studies Hybridoma Bank (DSHB), 1:10], mouse anti-Wingless (DSHB, 1:10), mouse anti-Myc (DSHB, 1:10), mouse anti-Discs large (DSHB, 1:10), rabbit anti-β-gal (1:1000, MP Biomedicals), and rabbit anti-GFP (1:500, Invitrogen). For secondaries, goat anti-mouse or anti-rabbit conjugated to either Alexa 488 or 555 (1:500; Invitrogen) were used. Fixed and stained embryos were carefully staged using head and gut morphology and individually mounted on glass coverslips in 60% glycerol. Confocal z-sections were obtained at ambient temperature on an inverted Olympus IX81 with a Crest CARV II confocal unit using a Plan VApo/340 60X/1.20 NA W objective and an ORCA-EM CCD Digital camera (Hamamatsu).

Cross-sections

Well slides for viewing embryos in cross section were prepared by painting small circles of valve lubricant (Dow Corning) on 24 × 60 mm^{2} rectangular coverslips. A solution of heptane and adhesive tape glue was applied in two layers, allowing the heptane to evaporate between applications. Stage 16 or 17 embryos were carefully staged using head and gut morphology and selected for dissection on a separate slide. Using a scalpel, a transverse cut was made through the entire diameter of each embryo approximately two-thirds of the way from the most anterior end; the section containing the most posterior end was then discarded. With the aid of a needle, each dissected embryo was propped up vertically on the

center of the well slide. A solution of 60% glycerol diluted in PBS was added drop-wise into the well, such that all embryos were completely immersed. The embryos were then imaged using an Olympus confocal microscope (described above). Statistical analysis was performed using GraphPad Prism.

Electron microscopy

Transmission electron microscopy was performed as described in (Soplop et al., 2009). Mutant embryos were selected based on the absence of GFP balancer in live dechorionated embryos prior to fixation.

Results and discussion

fra mRNA is expressed in the DV

fra encodes a transmembrane receptor for the Netrin guidance cue (Harris et al., 1996; Kolodziej et al., 1996; Mitchell et al., 1996). Previous studies have determined that *fra* is expressed in developing axons and epithelia in the *Drosophila* embryo ((Kolodziej et al., 1996). However, *fra* expression in the DV has not yet been reported. To determine whether *fra* mRNA was expressed in the DV, we performed in situ hybridization to embryos using a *fra* antisense probe. In addition to detecting the known expression of *fra* in the CNS and epidermal tissues (Kolodziej et al., 1996; Fig. 1), we also detected *fra* transcripts in the CBs as early as stage 14/15, with the transcript persisting in CBs in stage 16 embryos (Fig. 1A and B). We confirmed the CB expression of *fra* by double staining *Hand-Gal*4/*UAS-lacZ* embryos against *fra* mRNA and β-galactosidase (β-gal) protein. *Hand-Gal*4 drives expression in the CBs and a subset of the PCs (Han et al., 2006). Double staining confirmed that *fra* mRNA accumulates in all the CBs (Fig. 1C and D). We also detected *fra* mRNA in at least a subset of PCs (Fig. 1D).

Mutations in fra and Netrin cause DV defects

To investigate the potential role that *fra* plays during DV development, we examined embryos mutant for the *fra* gene in whole mount. In embryos homozygous for the molecularly characterized EMS-induced amorphic fra^3 allele (Kolodziej et al., 1996), we did not detect defects in the specification or overall number of CBs, as revealed by staining with anti-DMef2 (Fig. 1E and F), which labels the nuclei of all 104 CBs. In addition, Pericardin, a collagen-like protein that is secreted by the PCs and concentrates at the CB-pericardial cell interface (Chartier et al., 2002), was properly localized in fra^3 mutants (Fig. S1 B, C). While staining with anti-Wg, which labels the six bilateral pairs of CB ostial cells in the heart (Lo et al., 2002), showed that the ostial cells were correctly specified, Wg staining did reveal significant defects in the dorsal alignment of the two rows of CBs as seen by the shifting of the contralateral pairs of Wg positive CBs relative to each other (Fig. 1G and H). We observed this phenotype in 33% of fra^3 homozygotes, which was significantly above what we observed in wild type or $fra^3/+$ embryos ($P < 0.05$). The alignment phenotype, while mild, was also observed in the fra^4 allele (data not shown) and is also consistent with a previous study in which the authors isolated a new allele for *fra* in a genetic screen for heart malformations (Meyer et al., 2011).

To further investigate the defects we observed in *fra*^{3} mutants, we stained *fra*^{3} embryos with anti-αSpectrin (Lee et al., 1993), which labels CB lateral and luminal membranes. αSpectrin-staining in *fra*^{3} embryos confirmed the defects we observed in CB alignment and also revealed defects in CB attachment at the dorsal midline (Fig. 1J), without showing overall defects in CB polarity. Specifically, in 26% (*n*=35) of *fra*^{3} mutant embryos observed in whole mount, the dorsal-most membranes of opposing CBs did not appear to be properly attached, and we could see a space (spanning at least two or more cells) between opposing CBs (Fig. 1K). This attachment phenotype was not detected in wild type embryos. The defects in attachment did not appear to occur predominantly in specific cell types (i.e. the Wg-expressing ostial cells, which align with segment borders versus the sets of four pairs of Tinman-expressing cardioblasts (Gajewski et al., 2000) in between). In addition, we did not see gaps along the individual rows, suggesting that this defect is not in the dorsal migration of each row of CBs, but rather in the contact of CBs across the dorsal midline. Double staining with anti-DMef2 confirmed that these spaces were not due to the presence of extra CBs but most likely resulted from an attachment failure between contralateral CBs (Fig. 1L).

Fra is a known receptor for the secreted Netrin molecule, which is encoded by two genes, *NetrinA* (*NetA*) and *NetrinB* (*NetB*) in *Drosophila* (Harris et al., 1996; Kolodziej et al., 1996; Mitchell et al., 1996). While NetB protein has been reported to localize to the CBs (Albrecht et al., 2011; Harris et al., 1996), there are conflicting data in the literature regarding the source of secreted NetB in the CBs. While an early study reported weak *NetB* mRNA in the DV (Mitchell et al., 1996), a more recent study reported a failure to detect *NetB* transcript and suggested that NetB is diffusing from another source (Albrecht et al., 2011). In order to determine if the *fra*^{3} alignment and attachment defects we observed are downstream of Netrin signaling, we examined Δ*NetAB* embryos, in which both Netrin genes are specifically deleted by P-element excision (Brankatschk and Dickson, 2006). Staining with anti-Wg revealed occasional defects in CB alignment at the dorsal midline; however, the defects were not significantly above wild type levels (data not shown). Staining with anti-αSpectrin did reveal significant defects in CB attachment at the dorsal midline. Specifically, we found that 30% (*n*=23) of Δ*NetAB* embryos showed defects in CB attachment (Fig. 1M). These defects were similar to what we observed in *fra*^{3} mutants (Fig. 1K). Together, these results suggest that Netrin and Fra function together during DV formation in mediating CB attachment.

fra is required for CB attachment during DV morphogenesis

In order to more closely examine the roles of Fra and Netrin in the DV, embryos were cross-sectioned, which allowed us to visualize the specific contacts that are made by the CBs as well as the size and shape of the lumen. During morphogenesis of the DV, the rounded CBs undergo a series of cell shape changes, enabling first the dorsal and then the ventral region of each CB to initiate contact with their contralateral partner across the dorsal midline, while the areas in between remain unattached allowing for the formation of a lumen (Haag et al., 1999; Medioni et al., 2008; Santiago-Martinez et al., 2008).

We first cross-sectioned both wild type and *fra*^{3} embryos that were immunostained for αSpectrin to visualize CB membranes (see Materials and methods). In wild type embryos at

early stage 16, the dorsal-most contact between contralateral CBs has been established (Fig. 2A and A') and ventral contact is initiated. By stage 17, the CBs are attached at both dorsal and ventral attachment points and a lumen can be observed in between (Fig. 2B and B'). In *fra*^{3} mutants, we observed significant defects (85%, *n*=20) that arose from the failure of CBs to make appropriate contacts with each other across the dorsal midline at stage 17 (Table 1). We observed two main classes of phenotypes that range in severity. In the milder class, the CBs appeared to have undergone proper cell shape changes but then showed a missing or diminished area of dorsal and/or ventral contact, leading to an open-heart tube or a severely enlarged lumen (Fig. 2C and C'). In the second class, the CBs failed to undergo the cell shape changes required for CB outgrowth and as a result did not make either dorsal or ventral contact with each other across the dorsal midline (Fig. 2D, D'). In these sections, a clear space could be observed between the opposing CB membranes and we presume that this is the attachment phenotype that is clearly visible in our whole mount embryos (Fig. 1K and L). We confirmed that these embryos were not of an earlier stage or generally delayed in development by simultaneously examining head involution, gut morphology and dorsal closure with αSpectrin, which not only labels the CB membranes but also epidermal cells. We observed what appeared to be mild attachment defects in 31% of wild type embryos (Table 1), potentially reflecting that lumen formation does not simultaneously occur along the length of the embryo and that there are occasionally some CB pairs that have not completed the process at stage 17. However at this late stage in wild type embryos, we never observed a complete failure of CB outgrowth and the large space between contralateral CBs that we observed in *fra* mutants (Fig. 2D).

NetAB mutants share CB attachment phenotypes with fra mutants

In Δ*NetAB* mutants, the dominant phenotype was in CB attachment, similar to what we observed in *fra* mutants. Specifically, in 74% of the embryos we examined (*n*=19) (Table 1), contralateral CBs had either diminished attachment domains leading to an enlarged lumen (Fig. 2F and F') or a complete failure to attach (Fig. 2G and G'). We also observed a small number of embryos (5%) that showed CBs inappropriately attached along their entire luminal domain, resulting in a loss of lumen formation (Table 1). This phenotype was never observed in wild type embryos (Table 1), and is identical to the predominant phenotype we observed in *unc*5 loss-of-function embryos (36%, *n*=25) (Fig. 2I and I') (Table 1). This loss of lumen phenotype we observed in *unc*5 mutants as well as a small subset of *Netrin* mutants is consistent with the phenotypes reported in a recent study, which examined the role of *unc*5 during DV lumen formation (Albrecht et al., 2011). Together, these data demonstrate that Fra and Netrin function in mediating CB outgrowth and attachment and suggest, based on the phenotypes we observed, that this function may occur independently of Unc5-mediated CB repulsion.

fra and unc5 double mutants look like fra mutants

*unc*5 mutants fail to form a lumen due to a loss of repulsion leading to inappropriate contact between contralateral CBs (Albrecht et al., 2011; Fig. 2I and I'). This is in contrast to *fra* mutants in which there is a failure of contralateral CBs to make appropriate contact, presumably due to a loss of attraction (Fig. 2C and D). In order to determine the relative roles of these two opposing Netrin receptors, we examined *unc*5 and *fra* double-mutants and

found that the phenotype of the double mutant much more closely resembles the *fra* single-mutant phenotype (Fig. 2H, H'; Table 1) in which contralateral CBs fail to make contact at the dorsal midline. These data are consistent with the idea that *fra* functions prior to and independently of *unc*5 during lumen formation. This is further supported by our observation that Netrin mutants also predominantly display the *fra* mutant phenotype (Fig. 2F and G) and is consistent with previous studies showing that contralateral CBs must first initiate dorsal contacts before undergoing the cell shape changes leading to formation of the lumen (Haag et al., 1999; Medioni et al., 2008; Santiago-Martinez et al., 2008).

fra mutants show a loss of CB adhesion

Our results thus far are consistent with the idea that Fra is playing an important role in bringing together the CBs at specific sites of cell–cell contact. To more directly examine if cell contact and adhesion were specifically disrupted in *fra* mutants, we first performed EM analysis. Our EM data confirmed our analysis by cross-section. In fra^3 mutants, we often observed an enlarged luminal space between contralateral CBs, with the CB attachment domains severely decreased as compared to wild type (Fig. 3A and B). In contrast, *unc*5 mutants show CBs that are improperly attached at the luminal domain, resulting in a loss of lumen formation (Fig. 3C).

To further investigate whether *fra* mutants show a loss of CB cell contact, fra^3 mutant embryos were stained for the adhesion and junctional protein Discs-large (Dlg) (Woods et al., 1996). In $fra^3/+$ heterozygous embryos viewed in cross-section, Dlg localizes to the dorsal and ventral points of CB–CB contact as previously observed for wild type embryos (Medioni et al., 2008; Vanderploeg et al., 2012) (Fig. 3D). In fra^3 mutants, we see an absence of Dlg accumulation between CBs, indicating that the junctional domains did not properly form (Fig. 3E). In contrast, $unc5^8$ mutants showed an inappropriate accumulation of Dlg, consistent with the idea that CBs are adhered along the entire luminal domain, resulting in the absence of lumen formation (Fig. 3F).

Overexpression of fra leads to CB attachment defects

To further test the importance of *fra* in the DV, we performed a series of rescue and gain-of-function studies by driving a *UAS-fra* transgene in the DV with either the *Hand-Gal*4 or 24*B-Gal*4 drivers. Both *Hand-Gal*4 and 24*B-Gal*4 drive expression in the DV (Brand and Perrimon, 1993; Han et al., 2006). However, we found subtle but important differences between these drivers. First, *Hand-Gal*4 appears to drive expression in the CBs at lower levels than 24*B-Gal*4 (data not shown). Second, 24*B-Gal*4, which is known to reflect the expression of the *how* gene (Zaffran et al., 1997), does not drive expression uniformly in all CBs. For example, driving *UAS-mCD*8*-GFP* (a membrane-tethered fusion protein between mouse lymphocyte marker CD8 and the green fluorescence protein, (Lee and Luo, 1999) with 24*B-Gal*4 resulted in the accumulation of CD8-GFP at higher levels in the ostial CBs, which are aligned with segment borders, as compared with the sets of four pairs of contractile CBs in between (Fig. S2A).

We first attempted to rescue the *fra* mutant phenotype by driving *UAS-fra* in *fra* mutant embryos with either 24*B-Gal*4 or *Hand-Gal*4. We were not able to significantly rescue the

loss of CB attachment phenotype using either driver (Table 1). Furthermore, while driving expression of *UAS-fra* with the weaker *Hand-Gal*4 in an otherwise wild type background did not have an effect (Table 1), overexpression of *UAS-fra* at higher levels with 24*B-Gal*4 in wild type embryos resulted in significant CB attachment phenotypes, similar to what we observed in *fra* loss-of-function mutants (Table 1, Fig. 2E and E'). Interestingly, the *fra* gain-of-function phenotypes we observed with the 24*B-Gal*4 driver occurred at a much higher frequency between the ostial CBs, which show much higher levels of Fra-Myc expression (Fig. S2B) than the four pairs of contractile CBs in between (75% vs. 31% respectively). We were able to clearly identify the ostial CB cells in our cross-sections by their proximity to the alary muscles, which connect to the DV to support the cardiac tube as well as control hemolymph inflow (Bate, 1993; Rizki, 1978).

Together our results suggest that tight temporal and/or spatial regulation of Fra receptor levels in CBs is essential for the initiation and/or completion of the cell shape changes required for lumen formation, and that neither the 24*B-Gal*4 nor *Hand-Gal*4 drivers fully recapitulate normal levels of *fra* expression required for rescue of the attachment phenotypes in *fra* mutants. In addition, our overexpression data are consistent with findings in other systems that suggest that Fra function is highly regulated and that overexpression of *fra* often causes a disruption to its normal function, resulting in similar loss-of-function and gain-of-function phenotypes (Levy-Strumpf and Culotti, 2007; Timofeev et al., 2012; Watari-Goshima et al., 2007). An alternative interpretation of these results is that when *fra* is expressed at high levels in the CBs, it is able to function with Unc5 to mediate long-range repulsion, thus preventing the CBs from coming together. These data are supported by the findings that Unc5 functions as both a short-range and long-range repellent, and that only long-range repulsion requires Fra (Keleman and Dickson, 2001). In order to test this possibility, we overexpressed *fra* with 24*B-Gal*4 in embryos that were heterozygous for *unc*5. Interestingly, we found that *unc*5 was able to dominantly suppress the *fra* gain-of-function phenotype to near wild type levels (Table 1). These results are consistent with the idea that when expressed at high levels, *fra* can work in concert with *unc*5 to mediate long range repulsion of CBs, thus preventing CB attachment.

Fra localizes to sites of CB outgrowth and attachment

Our results thus far show that Fra functions in the CBs for proper outgrowth and attachment. Earlier studies have shown that the Fra homologs Unc-40 and DCC localize to distinct subcellular locations on the cell membrane, often in response to Netrin signaling (Adler et al., 2006; Matsumoto and Nagashima, 2010; Ziel et al., 2009). While our findings clearly showed that *fra* mRNA is expressed by the CBs (Fig. 1A–D), we were unable to detect endogenous Fra protein above background levels using an anti-Fra antibody previously used to localize the protein in the CNS (Garbe and Bashaw, 2007). As an alternative method to determine whether Fra protein has a specific subcellular distribution in the CBs, we examined the expression of the *UAS-fra-myc* transgene driven by either *Hand-Gal*4 or 24*B-Gal*4. In performing these experiments, we took advantage of the differences between the Hand and 24*B-Gal*4 drivers in our analysis. We first examined *Hand-Gal*4/*UAS-fra-myc* embryos stained with anti-Myc. Overexpression of *fra* using the *Hand-Gal*4 driver did not result in significant defects in CB attachment (Table 1). During the initial stages of DV

formation, as the CBs approached the midline, we were unable to detect high levels of Fra-Myc accumulation in CBs in these embryos (data not shown). However, at stage 17, when lumen formation was complete, we observed the accumulation of high levels of Fra-Myc at the sites of CB–CB contact (Fig. S3A).

To determine the localization of Fra in CBs at earlier stages, we examined *UAS-fra-myc* expression driven by the stronger 24*B-Gal*4 driver. A potential complication of using this driver to localize Fra is that overexpression of *UAS-fra* caused significant defects in CB attachment (Table 1, Fig. 2E). Because our subsequent analysis showed that these defects occurred much more frequently in the ostial CBs (see above), we initially focused our analysis on sections through the non-ostial CBs that showed a normal morphology. In these sections, we noticed that as contralateral CBs approached the dorsal midline at early stage 16, Fra-Myc staining became enriched first at the CB dorsal leading edge (Fig. 4A and A') and subsequently at the ventral leading edge (Fig. 4B and B'). Finally, at the completion of lumen formation at stage 17, Fra-Myc staining persisted at areas of CB contact (Fig. 4C and C'). As a control for our localization experiments, we used 24*B-Gal*4 to drive the expression of *UAS-mCD*8-*GFP*, a heterologous membrane protein. We found that unlike the highly localized pattern that we observed for Fra-Myc, the mCD8-GFP protein appeared to be evenly distributed along the surface of the CBs, as visualized with anti-GFP staining (Fig. S3B). These results are consistent with the idea that Fra localization specifically correlates with areas of CB membrane outgrowth and attachment.

We next questioned whether the attachment phenotype that we observed between CB ostial cells in *fra*-overexpressing embryos could be correlated with changes in Fra-Myc localization. We examined Fra-Myc localization in 24*B-Gal*4/*UAS-fra-Myc* embryos double-stained with anti-Wg, a marker for the CB ostial cells (Lo et al., 2002) and anti-Myc. We hypothesized that Wg-negative CBs expressing lower levels of *UAS-fra-Myc* would show normal CB morphology and by extension, the Fra-Myc staining would reflect a normal pattern of Fra localization. In contrast, we hypothesized that, higher levels of *UAS-fra-Myc* expression would lead to defects in CB attachment as well as mislocalization of Fra-Myc. As expected, we found that cross-sections through the high-*fra-Myc* expressing Wg positive ostial CBs clearly showed a more homogeneous distribution of Fra-Myc as well as significant CB attachment defects (Fig. 4D and E). In contrast, cross-sections through non-Wg expressing cells showed a more restricted distribution of Fra-Myc at sites of CB attachment and a normal lumen (Fig. 4F). We further confirmed this by examining additional cross-sections from a single embryo that we double stained with anti-Myc and anti-αSpectrin, to label the entire CB membrane (Fig. 4 G–L). In these sections, due to the lack of Wg staining, we identified the higher Fra-Myc expressing CB ostial cells by their proximity to the alary muscles. In sections taken through the CB ostial cells, we observed clear defects in CB morphogenesis together with a more homogeneous localization of Fra-Myc on the CB membrane (Fig. 4 G–I). In contrast, a neighboring section taken through a non-ostial CB shows accumulation of Fra-Myc at sites of CB outgrowth and attachment (Fig. 4J–L).

Together, these results support the idea that Fra accumulation at sites of CB outgrowth and adhesion is required for proper lumen formation. Our findings are consistent with previous

studies showing that Fra/Unc-40 becomes polarized on cell membranes that correspond to areas of cell outgrowth (Adler et al., 2006; Ziel et al., 2009). However, it is important to note that all of our observations are based on overexpression studies and therefore may not entirely reflect the localization of endogenous Fra protein in the DV.

Fra accumulation at sites of CB attachment is disrupted in Netrin mutants

Netrins have previously been shown to promote the recruitment of DCC/Fra to distinct locations of the cell membrane (Adler et al., 2006; Matsumoto and Nagashima, 2010). Furthermore, in the *Drosophila* CNS, Fra was shown to relocalize in response to Netrin signaling (Hiramoto et al., 2000). In the DV, both *fra* and *Netrin* mutants showed significant defects in CB attachment (Fig. 2 E and G, Table 1), suggesting that they function together during this process. To test whether the accumulation of Fra that we observed at specific points of CB attachment was dependent upon Netrin, we repeated our Fra-Myc localization studies described above in embryos that were heterozygous or homozygous for Δ*NetAB*. Because we observed Fra-Myc accumulation at sites of attachment specifically in the non-ostial CBs, we focused on these cells for our analysis. In Δ*NetAB*/+; 24*B-Gal*4/*UAS-fra-Myc* embryos, we detected Fra-Myc at points of CB attachment (Fig. 4M), similar to the pattern we saw in wild type embryos at stage 17 (Fig. 4C). However, in embryos homozygous for Δ*NetAB*, we often found that Fra-Myc staining was more diffusely distributed around the CB membrane or inappropriately accumulated at areas not normally associated with CB attachment (Fig. 4N). However, in some sections, we also observed normal distribution of Fra-Myc (Fig. 4O). Together, these findings support the idea that Fra localization at sites of attachment may at least be partially dependent upon Netrin signaling.

Conclusions

In this paper we have shown an important role for the Fra protein during DV formation. DV formation occurs via a series of highly stereotyped cell shape changes resulting in a linear tube comprising of two rows of CBs that are attached at their dorsal and ventral-most points, with a lumen in between (Fig. 5). Cell contact and adhesion is first initiated dorsally, as each CB extends a leading edge towards its contralateral counterpart across the dorsal midline, resulting in an adhesive interaction (Fig. 5B–C). By using loss-of-function analysis, we show that *fra* is required for this CB outgrowth. In addition, we show that Fra protein accumulates at sites of CB outgrowth and attachment (Fig. 5B–D) and that this localization of Fra can be correlated with proper CB morphogenesis. Overexpression of Fra at high levels results in a homogeneous distribution of Fra along the entire CB membrane leading to defects in CB attachment. Furthermore, we show that embryos mutant for both the *fra* and *unc*5 receptors or their common ligand Netrin primarily display a *fra* phenotype, demonstrating that *fra*-mediated CB outgrowth and attachment occurs prior to and largely independent of *unc*5-mediated lumen formation. Interestingly, the pattern of Fra is complementary to those reported for the Unc5 and Robo receptors, which are localized to the CB lumen where they are required for repulsion of CB membranes in order to form a luminal space (Fig. 5;Albrecht et al., 2011; Santiago-Martinez et al., 2008). We previously showed that overexpression of Robo results in inappropriate expansion of the luminal domain and a loss of CB–CB contact (Santiago-Martinez et al., 2008). Thus, CB

morphogenesis occurs by the sequential outgrowth and inhibition of discrete CB membrane domains. It is still unclear how these opposing signaling pathways are asymmetrically regulated inside the cell. Our findings together with the known localization patterns of Unc5 and Robo suggest that the localization of these receptors to discrete membrane domains is essential for proper CB morphogenesis.

Supplementary Material

Refer to Web version on PubMed Central for supplementary material.

Acknowledgments

We thank: Greg Bashaw, Barry Dickson and B. Paterson, Zhe Han for reagents, Rajesh Patel for assistance with EM, and members of the Wadsworth lab for helpful discussions. We would also like to acknowledge the Bloomington Stock Center at the Indiana University for providing fly stocks, and the Developmental Studies Hybridoma Bank developed under the auspices of the NICHD and maintained by The University of Iowa, Department of Biology for antibodies. This work was funded by NIH R01AR054482 from NIAMS for S.G.K. and a Rutgers/UMDNJ Biotechnology Training Grant T32 GM008339 for F.D.M.

References

Adler CE, Fetter RD, Bargmann CI. UNC-6/Netrin induces neuronal asymmetry and defines the site of axon formation. Nat Neurosci. 2006; 9:511–518. [PubMed: 16520734]

Albrecht S, Altenhein B, Paululat A. The transmembrane receptor Uncoordinated5 (Unc5) is essential for heart lumen formation in Drosophila melanogaster. Dev Biol. 2011; 350:89–100. [PubMed: 21094637]

Andrews GL, Tanglao S, Farmer WT, Morin S, Brotman S, Berberoglu MA, Price H, Fernandez GC, Mastick GS, Charron F, Kidd T. Dscam guides embryonic axons by Netrin-dependent and -independent functions. Development. 2008; 135:3839–3848. [PubMed: 18948420]

Brand AH, Perrimon N. Targeted gene expression as a means of altering cell fates and generating dominant phenotypes. Development. 1993; 118:401–415. [PubMed: 8223268]

Brankatschk M, Dickson BJ. Netrins guide Drosophila commissural axons at short range. Nat Neurosci. 2006; 9:188–194. [PubMed: 16429137]

Chartier A, Zaffran S, Astier M, Semeriva M, Gratecos D. Pericardin, a Drosophila type IV collagen-like protein is involved in the morphogenesis and maintenance of the heart epithelium during dorsal ectoderm closure. Development. 2002; 129:3241–3253. [PubMed: 12070098]

Gajewski K, Choi CY, Kim Y, Schulz RA. Genetically distinct cardial cells within the Drosophila heart. Genesis. 2000; 28:36–43. [PubMed: 11020715]

Garbe DS, Bashaw GJ. Independent functions of Slit-Robo repulsion and Netrin-Frazzled attraction regulate axon crossing at the midline in Drosophila. J Neurosci. 2007; 27:3584–3592. [PubMed: 17392474]

Haag TA, Haag NP, Lekven AC, Hartenstein V. The role of cell adhesion molecules in Drosophila heart morphogenesis: faint sausage, shotgun/DE-cadherin, and laminin A are required for discrete stages in heart development. Dev Biol. 1999; 208:56–69. [PubMed: 10075841]

Han Z, Yi P, Li X, Olson EN. Hand, an evolutionarily conserved bHLH transcription factor required for Drosophila cardiogenesis and hematopoiesis. Development. 2006; 133:1175–1182. [PubMed: 16467358]

Harris R, Sabatelli LM, Seeger MA. Guidance cues at the Drosophila CNS midline: identification and characterization of two Drosophila Netrin/UNC-6 homologs. Neuron. 1996; 17:217–228. [PubMed: 8780646]

Hiramoto M, Hiromi Y, Giniger E, Hotta Y. The Drosophila Netrin receptor Frazzled guides axons by controlling Netrin distribution. Nature. 2000; 406:886–889. [PubMed: 10972289]

Ishii N, Wadsworth WG, Stern BD, Culotti JG, Hedgecock EM. UNC-6, a laminin-related protein, guides cell and pioneer axon migrations in *C. elegans*. Neuron. 1992; 9:873–881. [PubMed: 1329863]

Keleman K, Dickson BJ. Short- and long-range repulsion by the Drosophila Unc5 netrin receptor. Neuron. 2001; 32:605–617. [PubMed: 11719202]

Kolodziej PA, Timpe LC, Mitchell KJ, Fried SR, Goodman CS, Jan LY, Jan YN. frazzled encodes a Drosophila member of the DCC immunoglobulin subfamily and is required for CNS and motor axon guidance. Cell. 1996; 87:197–204. [PubMed: 8861904]

Labrador JP, O'Keefe D, Yoshikawa S, McKinnon RD, Thomas JB, Bashaw GJ. The homeobox transcription factor even-skipped regulates netrin-receptor expression to control dorsal motor-axon projections in Drosophila. Curr Biol. 2005; 15:1413–1419. [PubMed: 16085495]

Lai Wing Sun K, Correia JP, Kennedy TE. Netrins: versatile extracellular cues with diverse functions. Development. 2011; 138:2153–2169. [PubMed: 21558366]

Lecuyer, E.; Necakov, AS.; Caceres, L.; Krause, HM. High-resolution fluorescent in situ hybridization of Drosophila embryos and tissues. Cold Spring Harb Protoc. 2008. http://dx.doi.org/10.1101/pdb.prot5019

Lee JK, Coyne RS, Dubreuil RR, Goldstein LS, Branton D. Cell shape and interaction defects in alpha-spectrin mutants of *Drosophila melanogaster*. J Cell Biol. 1993; 123:1797–1809. [PubMed: 8276898]

Lee T, Luo L. Mosaic analysis with a repressible cell marker for studies of gene function in neuronal morphogenesis. Neuron. 1999; 22:451–461. [PubMed: 10197526]

Levy-Strumpf N, Culotti JG. VAB-8, UNC-73 and MIG-2 regulate axon polarity and cell migration functions of UNC-40 in *C. elegans*. Nat Neurosci. 2007; 10:161–168. [PubMed: 17237777]

Lo PC, Skeath JB, Gajewski K, Schulz RA, Frasch M. Homeotic genes autonomously specify the anteroposterior subdivision of the Drosophila dorsal vessel into aorta and heart. Dev Biol. 2002; 251:307–319. [PubMed: 12435360]

Ly A, Nikolaev A, Suresh G, Zheng Y, Tessier-Lavigne M, Stein E. DSCAM is a netrin receptor that collaborates with DCC in mediating turning responses to netrin-1. Cell. 2008; 133:1241–1254. [PubMed: 18585357]

Matsumoto H, Nagashima M. Netrin-1 elevates the level and induces cluster formation of its receptor DCC at the surface of cortical axon shafts in an exocytosis-dependent manner. Neurosci Res. 2010; 67:99–107. [PubMed: 20170691]

Medioni C, Astier M, Zmojdzian M, Jagla K, Semeriva M. Genetic control of cell morphogenesis during Drosophila melanogaster cardiac tube formation. J Cell Biol. 2008; 182:249–261. [PubMed: 18663140]

Meyer H, Panz M, Albrecht S, Drechsler M, Wang S, Husken M, Lehmacher C, Paululat A. Drosophila metalloproteases in development and differentiation: the role of ADAM proteins and their relatives. Eur J Cell Biol. 2011; 90:770–778. [PubMed: 21684629]

Mitchell KJ, Doyle JL, Serafini T, Kennedy TE, Tessier-Lavigne M, Goodman CS, Dickson BJ. Genetic analysis of Netrin genes in Drosophila: Netrins guide CNS commissural axons and peripheral motor axons. Neuron. 1996; 17:203–215. [PubMed: 8780645]

Molina MR, Cripps RM. Ostia, the inflow tracts of the Drosophila heart, develop from a genetically distinct subset of cardial cells. Mech Dev. 2001; 109:51–59. [PubMed: 11677052]

Moore SW, Tessier-Lavigne M, Kennedy TE. Netrins and their receptors. Adv Exp Med Biol. 2007; 621:17–31. [PubMed: 18269208]

Purohit AA, Li W, Qu C, Dwyer T, Shao Q, Guan KL, Liu G. Down Syndrome Cell Adhesion Molecule (DSCAM) associates with uncoordinated-5C (UNC5C) in Netrin-1-mediated growth cone collapse. J Biol Chem. 2012; 287:27126–27138. [PubMed: 22685302]

Quinn CC, Wadsworth WG. Axon guidance: asymmetric signaling orients polarized outgrowth. Trends Cell Biol. 2008; 18:597–603. [PubMed: 18951796]

Santiago-Martinez E, Soplop NH, Patel R, Kramer SG. Repulsion by Slit and Roundabout prevents Shotgun/E-cadherin-mediated cell adhesion during Drosophila heart tube lumen formation. J Cell Biol. 2008; 182:241–248. [PubMed: 18663139]

Soplop NH, Patel R, Kramer SG. Preparation of embryos for electron microscopy of the Drosophila embryonic heart tube. J Vis Exp. 2009

Timofeev K, Joly W, Hadjieconomou D, Salecker I. Localized netrins act as positional cues to control layer-specific targeting of photoreceptor axons in Drosophila. Neuron. 2012; 75:80–93. [PubMed: 22794263]

Vanderploeg J, Vazquez Paz LL, MacMullin A, Jacobs JR. Integrins are required for cardioblast polarisation in Drosophila. BMC Dev Biol. 2012; 12:8. [PubMed: 22353787]

Watari-Goshima N, Ogura K, Wolf FW, Goshima Y, Garriga G. *C. elegans* VAB-8 and UNC-73 regulate the SAX-3 receptor to direct cell and growth-cone migrations. Nat Neurosci. 2007; 10:169–176. [PubMed: 17237778]

Woods DF, Hough C, Peel D, Callaini G, Bryant PJ. Dlg protein is required for junction structure, cell polarity, and proliferation control in Drosophila epithelia. J Cell Biol. 1996; 134:1469–1482. [PubMed: 8830775]

Xu Z, Li H, Wadsworth WG. The roles of multiple UNC-40 (DCC) receptor-mediated signals in determining neuronal asymmetry induced by the UNC-6 (netrin) ligand. Genetics. 2009; 183:941–949. [PubMed: 19704011]

Zaffran S, Astier M, Gratecos D, Semeriva M. The held out wings (how) Drosophila gene encodes a putative RNA-binding protein involved in the control of muscular and cardiac activity. Development. 1997; 124:2087–2098. [PubMed: 9169854]

Ziel JW, Hagedorn EJ, Audhya A, Sherwood DR. UNC-6 (netrin) orients the invasive membrane of the anchor cell in *C. elegans*. Nat Cell Biol. 2009; 11:183–189. [PubMed: 19098902]

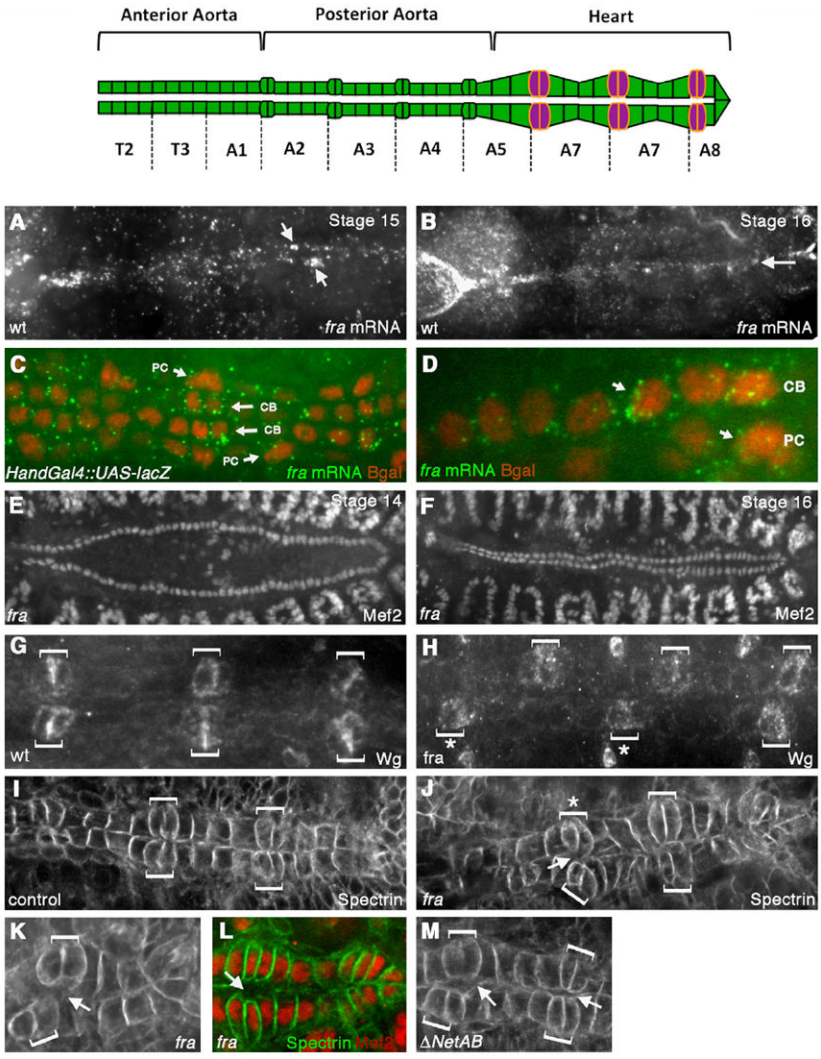

Fig. 1.

fra is expressed in the dorsal vessel and *fra* mutants have defects in CB alignment and attachment. Top panel shows a schematic of the embryonic DV, which spans segments T2–A8 and is divided into the anterior aorta, posterior aorta and the heart. In the heart, the six pairs of Wingless-expressing CB ostial cells are indicated in magenta. (A, B) In situ hybridization was performed with a DIG-labeled *fra* antisense probe and visualized using Tyramide signal amplification. Expression of *fra* at stage 15 is highly enriched in the DV (A). *fra* expression persists through stage 16 (B). (C, D) Co-staining *Hand-Gal4*/*UAS-lacZ* embryos for *fra* mRNA (green) and β-gal (red) shows the expression of *fra* mRNA on both the CBs and PCs (arrows). (E-F) anti-DMef2 staining in fra^3 mutants at stage 14 (E) and 16 (F) showing that CB specification and migration to the dorsal midline is not impaired in fra^3 mutants. Wild type embryos have 104 CBs, and we found no significant difference in CB number in fra^3 mutants (104+/−2, *n*=5). (G-H) Staining with anti-Wingless (Wg) in wild type (wt) (G) or fra^3 mutant (H) reveals that the ostial cells (brackets) are correctly specified in fra^3 mutants, but are often misaligned across the dorsal midline (asterisks). (I-J) anti-αSpectrin staining in the heart region of the DV. In wild type stage 16 embryos, the ostial

cells (brackets) are aligned with each other and make contact across the dorsal midline (I). In *fra*^{3} mutants (J), ostial cells (brackets) are often mis-aligned (asterisk) and fail to make proper contact with their contralateral counterparts (arrows). (K) Another *fra*^{3} mutant embryo showing mis-aligned CB ostial cells (brackets) and failure of CBs to make contact across the dorsal midline (arrow). (L) *fra*^{3} embryo double stained with anti-DMef2 (red) and anti-αSpectrin (green) to show that the space between CBs is not due to the presence of an extra CB. (M) Δ*NetAB* mutant embryos also show defects in CB attachment (arrows).

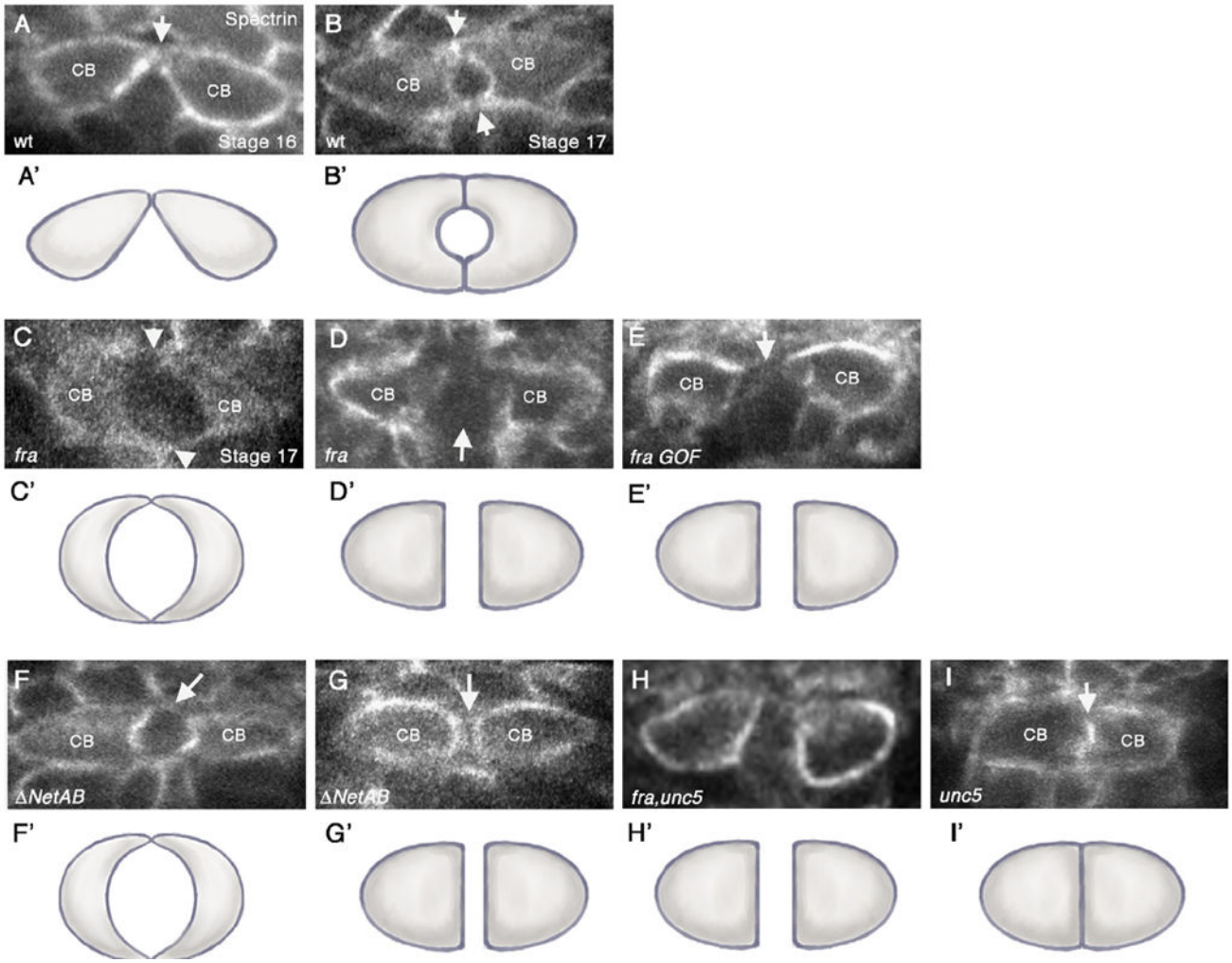

Fig. 2.

frazzled and *Netrin* mutants have defects in CB attachment. (A–I) Cross-sections taken through the heart region of the DV (abdominal segments A6–A8) of embryos immunostained with anti-αSpectrin, which outlines the CB membranes. Variances in αSpectrin staining between panels do not necessarily reflect differences in αSpectrin localization but rather in image processing. Except for panel (A), all embryos shown are at stage 17. (A'–I') are representative cartoons showing the shape of the CBs based on the cross-sections in the corresponding figures. (A, B) wild type (wt) embryos. (A) In early stage 16 wt embryos, contralateral CBs initiate contact at their dorsal-most regions (arrow). (B) By stage 17, both dorsal and ventral contacts have formed (arrows), and a lumen can be observed in between. (C). *fra*^{3} mutants show a range of lumen defects (C and D). (C) Diminished adhesion domain phenotype where dorsal and ventral contacts appear to form (arrowheads) but are severely diminished compared to wt. In addition, the lumen appears enlarged. (D) Arrested phenotype, where CBs migrate to the dorsal midline, but then fail to undergo further cell shape changes resulting in a large space in between contralateral CBs (arrow). (E) Overexpression of *UAS-fra* at high levels in CBs with 24*B-Gal*4 results in an "arrest" phenotype, where the CBs have failed to initiate dorsal contact (arrow). (F, G) In

Δ*NetAB* embryos, the attachment points between CBs are often diminished or absent (arrows) (F) or CBs fail to undergo cell shape changes leading to failure to make contact (arrow) (G). (H) *unc*5, *fra* double mutants show an "arrest" phenotype in which the CBs fail to make contact. (I) In *unc*5^{8} mutants, we observed inappropriate attachment of CBs (arrow) resulting in a no-lumen phenotype.

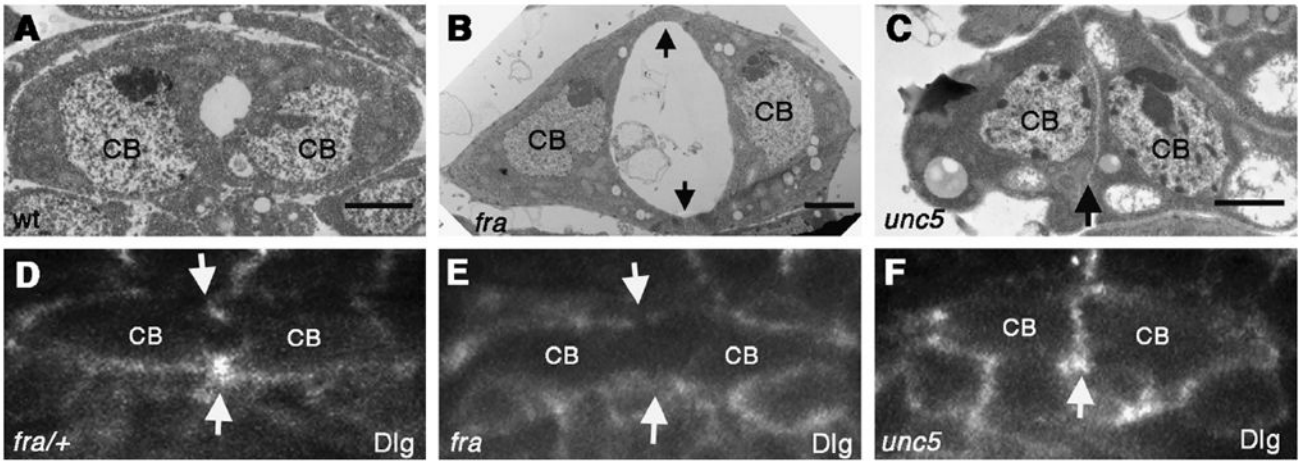

Fig. 3.

fra mutants show diminished adherent domains. TEM sections through the heart of stage 17 wild type (wt) (A), *fra*^{3} and *unc5*^{8} mutant embryos (B) and (C) respectively. In *fra*^{3} mutants (B) the area of CB–CB contact is diminished (arrows) and the lumen appears enlarged as compared with wt. In contrast, unc5 mutants (C) are inappropriately adhered along the entire CB face, resulting in the absence of a lumen (arrow). In *fra*^{3}/+ heterozygotes, Discs large (Dlg), a junctional marker is enriched at the dorsal and ventral sites of CB contact (arrows) (D). In *fra*^{3}/ *fra*^{3} embryos, Dlg fails to accumulate at these points (arrows) (E). In *unc*5^8 mutants, Dlg accumulates between CBs that are inappropriately attached (F).

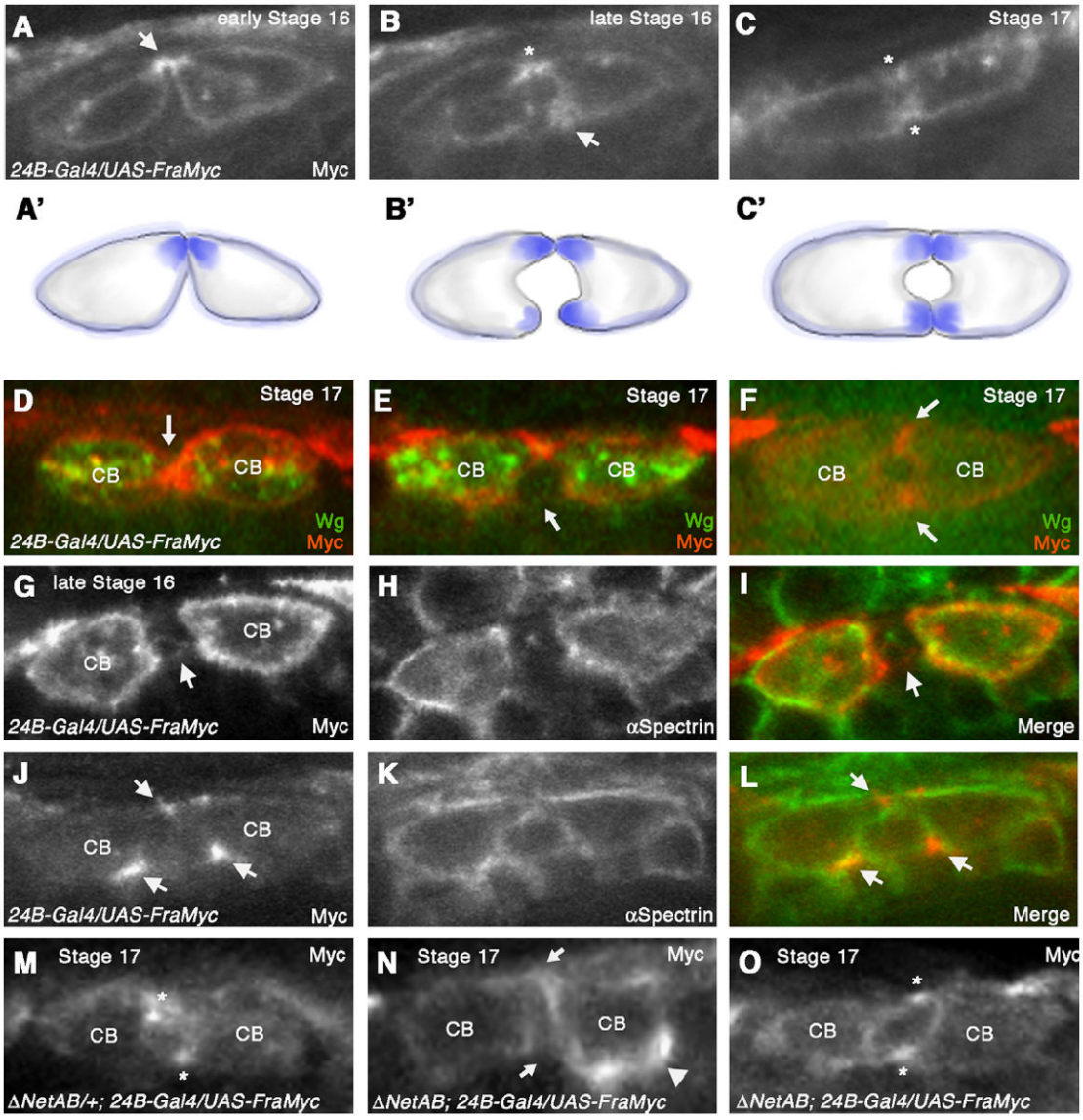

Fig. 4.

Frazzled protein concentrates at sites of CB attachment (A–C) Cross-sections of embryos expressing *UAS-fra-Myc* in all CBs with 24*B-Gal*4. (A) Anti-Myc staining at early stage 16 reveals that Fra-Myc accumulates dorsally in the CBs corresponding to the initial sites of contact (arrow). (B) At late stage 16, Fra-Myc also accumulates at the site of ventral CB outgrowth (arrow). Dorsal contact is indicated with an asterisk. (C) Stage 17 embryo when lumen formation is complete. Fra-Myc staining persists at dorsal and ventral sites of contact (asterisks). Schematic diagrams illustrating Fra-Myc localization (A'–C'). (D, F) Double labeling of *UAS-fra-Myc*/24*B-Gal*4 embryo with anti Myc and anti-Wg, which labels the 6 pairs of ostial CBs in the heart. CBs that were Wg positive showed CB attachment phenotypes as well as uniform distribution of Fra-Myc (D and E). In CBs that were negative for Wg protein (F), Fra-Myc accumulated at dorsal and ventral points of attachment (arrows) and the lumen appeared normal. (G-I) *UAS-fra-myc*/24*B-Gal*4 embryo sectioned through the

ostial CBs, which express high levels of Fra-Myc. In these embryos, Fra-Myc staining (G) was evenly distributed along the entire CB membrane, similar to αSpectrin (H). (I) is a merge of (G) and (H). (J–L) *UAS-fra-myc*/24*B*-*Gal*4 embryo sectioned through the non-ostial CBs expressing lower levels of fra-Myc. Arrows point to the areas that accumulate Fra-Myc protein. (L) is a merge of (J) and (K). (M–O) (M) Fra-Myc accumulates at dorsal and ventral attachment points (asterisks) in a Δ*NetAB* heterozygote at stage 17. (N) In a Δ*NetAB* mutant, Fra-Myc accumulation at these sites is disrupted (arrows) and we observe inappropriate accumulation of Fra-Myc on areas of the CB membrane not normally associated with attachment (arrowhead). In these sections a proper lumen fails to form. (O) In Δ*NetAB* mutants that show a normal lumen, we also observe normal distribution of Fra-Myc (asterisks).

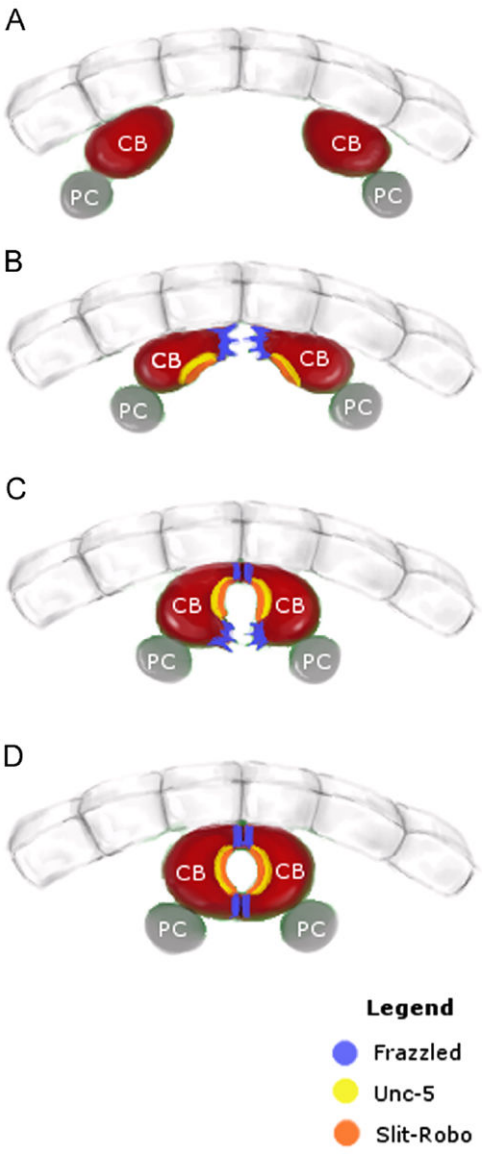

Fig. 5.

Summary of the roles of Frazzled, Unc-5 and Slit/Robo during dorsal vessel morphogenesis. Schematic showing four stages of dorsal vessel morphogenesis as visualized in cross-section. Panel (A) shows contralateral cardioblasts (CBs, red) as they are migrating towards the dorsal midline. (B) As they approach the midline, contralateral CBs extend their dorsal-most membrane regions. These membrane domains accumulate Frazzled protein (blue). (C) Following contact of the dorsal membranes, CBs extend their Frazzled-rich ventral membranes, while the regions in-between remain unattached due to Slit/Robo (orange) and Unc-5 (yellow) signaling. (D) Closure of the dorsal vessel showing Frazzled protein persisting at dorsal and ventral contact points. (For interpretation of the references to color in this figure legend, the reader is reffered to the web version of this article.)

Table 1

Quantification of CB phenotypes in cross-sectioned embryos.

	No defect	Defect in CB–CB contact	No lumen
wt	69% (20/29)	31% (9/29)	0% (0/29)
fra^{3}	15% (3/20)	85% (17/20)[a]	0% (0/20)
Δ*NetAB*	21% (4/19)	74% (14/19)[a]	5% (1/19)
unc5^{8}	36% (9/25)	28% (7/25)	36% (9/25)[a]
unc5^{GS},*fra*^{3}	30% (6/20)	70% (14/20)[a]	0% (0/20)
fra^{3}; *UAS-fra X Hand-Gal4*	27% (4/15)	73% (11/15)[a]	0% (0/15)
fra^{3}; *UAS-fra X* 24*B-Gal*4	27% (6/22)	73% (16/22)[a]	0% (0/22)
UAS-fra X *Hand-Gal*4	74% (17/23)	26% (6/23)	0% (0/23)
UAS-fra X 24*B-Gal*4	32% (7/22)	68% (15/22)[a]	0% (0/22)
unc5^{8}/+; *UAS-fra* X 24*B-Gal*4	65% (13/20)	35% (7/20)	0% (0/20)

[a] Data sets differ significantly from WT with a P value of <0.05 by the T-test.